Journal of Astronomical Telescopes, Instruments, and Systems

AstronomicalTelescopes.SPIEDigitalLibrary.org

Development of imaging x-ray telescopes at Tongji University

Zhanshan Wang
Yingyu Liao
Zhengxiang Shen
Qiushi Huang
Bin Ma
Zhong Zhang
Xiaoqiang Wang
Kun Wang
Jun Yu
Shenghao Chen
Zhenbo Wei
Shuang Ma
Yang Yang
Chun Xie
Vadim Burwitz

SPIE.

Zhanshan Wang, Yingyu Liao, Zhengxiang Shen, Qiushi Huang, Bin Ma, Zhong Zhang, Xiaoqiang Wang, Kun Wang, Jun Yu, Shenghao Chen, Zhenbo Wei, Shuang Ma, Yang Yang, Chun Xie, Vadim Burwitz, "Development of imaging x-ray telescopes at Tongji University," *J. Astron. Telesc. Instrum. Syst.* **5**(4), 044010 (2019), doi: 10.1117/1.JATIS.5.4.044010.

Development of imaging x-ray telescopes at Tongji University

Zhanshan Wang,[a,b,*] Yingyu Liao,[a,b] Zhengxiang Shen,[a,b] Qiushi Huang,[a,b] Bin Ma,[a,b] Zhong Zhang,[a,b] Xiaoqiang Wang,[a,b] Kun Wang,[c] Jun Yu,[a,b] Shenghao Chen,[a,b] Zhenbo Wei,[a,b] Shuang Ma,[a,b] Yang Yang,[a,b] Chun Xie,[d] and Vadim Burwitz[e]

[a]Ministry of Education, Tongji University, Key Laboratory of Advanced Micro-Structured Materials, Shanghai, China
[b]Tongji University, Institute of Precision Optical Engineering, School of Physics Science and Engineering, Shanghai, China
[c]Tongji University, School of Mechanical Engineering, Shanghai, China
[d]Tongji University, Sino-German College of Applied Sciences, Shanghai, China
[e]Max-Planck-Institute for Extraterrestrial Physics, Garching, Germany

Abstract. The imaging x-ray telescope (IXT) was first developed at the Institute of Precision Optical Engineering of Tongji University in 2007. Since then, we have made great progress on the development of mirror fabrication, coatings, and optic assembly. In this paper, we intend to provide an overview of the progress. Currently, we can routinely produce cylindrical mirror substrates with angular resolution of 30″ to 60″. To improve the effective area, coatings using C, Ni, and Pt layers were designed and achieved a high reflectivity at 0.5 to 10 keV. During the optic assembly, an *in-situ* measurement system and a three-dimensional ray-tracing program have been developed, thus guiding the assembly process in real time. Several prototypes have been fabricated, and one of them with 21 mirror layers was calibrated at the MPE PANTER x-ray test facility in Germany. The IXT prototype, with a focal length of 2052.5 mm, is characterized by a measured half-power diameter of 111″ and effective area of 39 cm^2 at 1.49 keV. [DOI: 10.1117/1.JATIS.5.4.044010]

Keywords: imaging x-ray telescope; thermal slumping technology; coatings; telescope assembly; ray-tracing program; x-ray calibration.

Paper 19043 received Apr. 24, 2019; accepted for publication Nov. 18, 2019; published online Dec. 6, 2019.

1 Introduction

The x-ray universe teems with transients and variable objects providing people with lots of information to explore the limits of contemporary physics and to study matter under extreme conditions. With the development of grazing incidence telescopes, x-ray astronomy has become a major branch of astrophysics. Specially, the Wolter-I configuration has been considered to be crucial in the development of grazing incidence optics. The Wolter-I configuration, consisting of a coaxial, confocal paraboloid and hyperboloid, was first proposed by Wolter.[1] X-ray telescopes using Wolter-I configuration were proposed by Giacconi and Rossi.[2] To obtain large collecting area, a nested Wolter-I configuration was described by VanSpeybroeck and Chase.[3] Petre and Serlemitsos[4,5] designed a conical Wolter-I configuration. They approximated the parabola and hyperbola surface of the Wolter-I configuration with double cones. This solution could greatly reduce the cost and difficulty of mirror fabrication at the expense of angular resolution. Since then, Wolter-I configuration and its optimization solutions[6–8] have been intensively researched and became the model for imaging x-ray telescopes (IXTs). For instance, the Chandra telescope[9] features an unprecedented angular resolution of 0.5″ and the XMM-Newton telescope[10] possesses a large effective area of over 4000 cm^2 at 1.5 keV. As the first focusing high-energy x-ray mission, the NuSTAR telescope[11] opened the hard x-ray sky above 10 keV for sensitive study, by utilizing the thermal slumping technology and depth-graded multilayers.

China has made tremendous achievement in non-IXTs, which is the well-known hard x-ray modulation telescope (Insight-HXMT).[12] However, even though IXTs have been developed for half a century, China has not been involved in international cooperation to fabricate IXTs in Wolter-I configuration. Lack of core technology encouraged us to strengthen international cooperation, meanwhile, developing IXT on our own. For over the past 10 years, China has proposed and is currently leading several IXT missions. The X-ray Timing and Polarization satellite[13] and the enhanced X-ray Timing and Polarimetry[14] are proposed as the successors of the Insight-HXMT, dedicated to study black hole, neutron star, and then get more information in the physics under extreme gravity, density, and magnetism. The Einstein Probe[15] mission aims at discovering transients and monitoring variable objects in the 0.5 to 4 keV x-rays, at a sensitivity higher by 1 order of magnitude than those of missions currently in orbit. The Hot Universe Baryon Surveyor (HUBS) mission is primarily to conduct a census of baryons in the warm-hot intergalactic media, thus directly addressing the issue of "missing baryons" in the local universe. The results are expected to impact our understanding of galaxy formation.

To develop IXTs independently, both faculty and students of the Institute of Precision Optical Engineering (IPOE) of Tongji University have been studying and testing thermal slumping technology since 2007.[16–18] Thermal slumping technology, i.e., the copying of the figure of a precision-polished mandrel onto a thin sheet of glass, was first applied in an experimental Kirkpatrick-Baez telescope for extreme ultraviolet and soft x-ray band.[19] The use of reusable high-precision mandrels makes the thermal slumping technology a low-cost way of producing mirror substrates. The continuing development of the

*Address all correspondence to Zhanshan Wang, E-mail: wangzs@tongji.edu.cn

Table 1 Brief introduction of mirror fabrication technology.

Technology	Mechanism	X-ray telescopes
Figuring and polishing	Finely figured and polished Zerodur or fused silicon.	Einstein, ROSAT, Chandra[22–24]
Aluminum epoxy replication[25]	The aluminum foil, heat-formed and sized, is prepared to a desired conical shape of which the radius is approximately the same radius of curvature to the mandrel. The prepared foil and the coated mandrel are sprayed separately with the epoxy before being put together inside a vacuum chamber.	ASTRO-E, Suzaku, ASTRO-H, NICER[26–28]
Electroforming replication[29,30]	Electroform nickel onto coated mandrel and separate the coated nickel substrate from the mandrel by cooling.	BeppoSAX, XMM-Newton, eROSITA, SWIFT[10,31–33]
Thermal slumping[34,35]	Thin glass sheets replicate the surface figure of the mandrel using high temperatures and gravity. The mirrors are coated after thermal slumping.	NuSTAR[11]
SPO[36]	After a series of processes applied to Si wafers, i.e., dicing, ribbing, wedging, and coating, the silicon mirrors are automatically stacked by machine without glue.	ATHENA[36]
PSO[37]	A polished mirror is sliced from a block of silicon followed by an etching, polishing, cutting, lightweight process.	STAR-X, Lynx[38,39]

process has led to a steady improvement in the angular resolution, making thermal slumping a promising way of fabricating IXTs with both high effective area and decent angular resolution, and at the same time lightweight and low cost.

However, it is the conical Wolter-I configuration that the IXT employs by utilizing thermal slumping technology. The imaging performance is inevitably degraded because of the double-cone geometry, which posed a challenge as the need to suppress the effect of this conic error. By increasing the focal length, the adverse effect can be effectively suppressed. Nevertheless, we focus on the research of IXT characterized by short focal length of ∼2 m, catering to the requirement of HUBS mission. For the purpose of verification, the very first prototype has been successfully integrated in 2016.[17] Subsequently, the optical and mechanical tests have been successfully performed. Ideally, the value of the on-axis half-power diameter (HPD) of an x-ray telescope in conically approximated Wolter-I geometry is about inversely proportional to the square of the focal length. The imaging performance could be improved by lengthening the focal length. However, with various errors taken into account, especially the figure error, this improvement could be restricted. In the past two years, we have made a great improvement in thermal slumping technology, coating fabrication, telescopes assembly, and assessment. The great progress in the development of short-focal-length IXT confirmed our ability to fabricate long-focal-length IXT with much better performance. In addition, we proposed two optimized geometries to improve the IXT performance, which are a hybrid configuration and a sectioned configuration.[20,21] The hybrid configuration uses one conical surface and one quadratic surface, while the sectioned configuration is a conical Wolter-I configuration with sectioned secondary mirrors.

This paper intends to provide an overview of the current progress of x-ray telescope fabrication at IPOE, Tongji University. In the following sections, the progress in thermal slumping technology is introduced. The fabrication of mirror coatings and the assembly of telescopes will follow. Lastly, we present the design, simulation, and calibration of the latest prototype, which was tested at the PANTER x-ray test facility of the Max-Planck Institute for Extraterrestrial Physics, Germany.

2 Thermal Slumping Technology

Optimized mirror fabrication technology is the prerequisite to produce high-performance x-ray telescopes. Apart from the thermal slumping technology, there are many other technologies used to fabricate x-ray mirrors, which include the figuring and polishing, electroforming replication, aluminum epoxy replication, Silicon Pore Optics (SPO), and newly developed Polished Silicon Optics (PSO). A brief summary of these technologies is given in Table 1.

As for the thermal slumping technology, thin glass sheets are utilized as mirror substrates, which have advantages in mass, volume, and cost. After ultrasonic cleaning, the glass sheet is put on a precisely figured and polished mandrel in an oven. By means of high temperature and gravity, the glass sheet can replicate the surface figure of the mandrel, as shown in Fig. 1. The mandrel is made of fused quartz, with its surface coated with a release layer.[40] The release layer prevents the glass sheet from adhering to the mandrel surface. In addition, it works as a lubricating interfacial layer between mandrel and glass sheets so

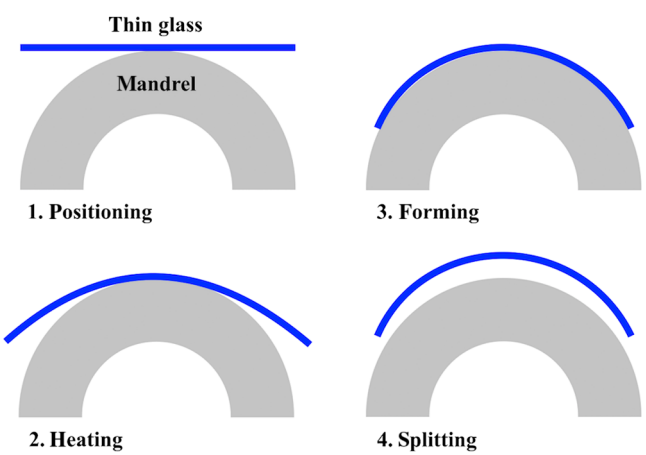

Fig. 1 Illustration of the thermal slumping process. The glass sheet inherits the surface figure of the mandrel by means of high temperature and gravity.

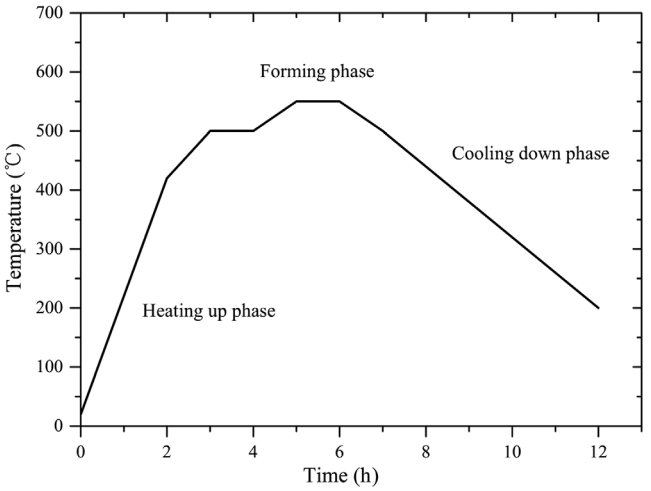

Fig. 2 Example of the temperature curve for thermal slumping technology, which ensures that the glass sheet replicate the surface figure of the mandrel as accurately as possible.

that the glass sheet can be separated from the mandrel freely after thermal slumping.

Proper temperature curves of the oven are set for corresponding mirrors with various radii, which ensure that the glass replicates the surface figure of the mandrel as accurately as possible. An example of the temperature curve is shown in Fig. 2. The thermal-slumped glasses are usually much larger than needed. Therefore, they are cut to required dimensions by utilizing a hot wire.[41] Metrology is also crucial for mirror fabrication. The low-frequency error is measured by using laser scanner and interferometer with the computer-generated hologram (CGH), and the high-frequency error is measured by utilizing an optical profilometer and an atomic force microscope (AFM).

The mandrels we use are cylindrical, similar to the NuSTAR ones, and one mandrel could cover 1 to 2 sizes of mirror substrates. Hence, large numbers of mandrels are needed to fabricate mirrors with various radii for an x-ray telescope with large diameter as HUBS required. The mandrels produced by the company Media Lario (Italy) are indeed of a very high quality. In the long term, the mandrels made in China will be an alternative. The Chinese mandrels have improved a lot in axial peak-to-valley value, giving it a value of <1 μm, even better than those from Media Lario. However, in terms of uniformity over the azimuth angle, the mandrels from Media Lario are better.

The best mandrel has a figure accuracy of 15″, which is the slope error with a sampling length of 0.7 mm relative to the cylindrical surface. To measure the surface of the cylindrical mandrel, an interferometer is utilized and the cylindrical wave is converted from the plane wave using the CGH. Apart from mandrels, the thermal slumping technology has made a great improvement by optimizing the temperature curves. Among the slumped mirrors, the best one is characterized by a figure accuracy of 21″. The laser scanner was developed by Columbia

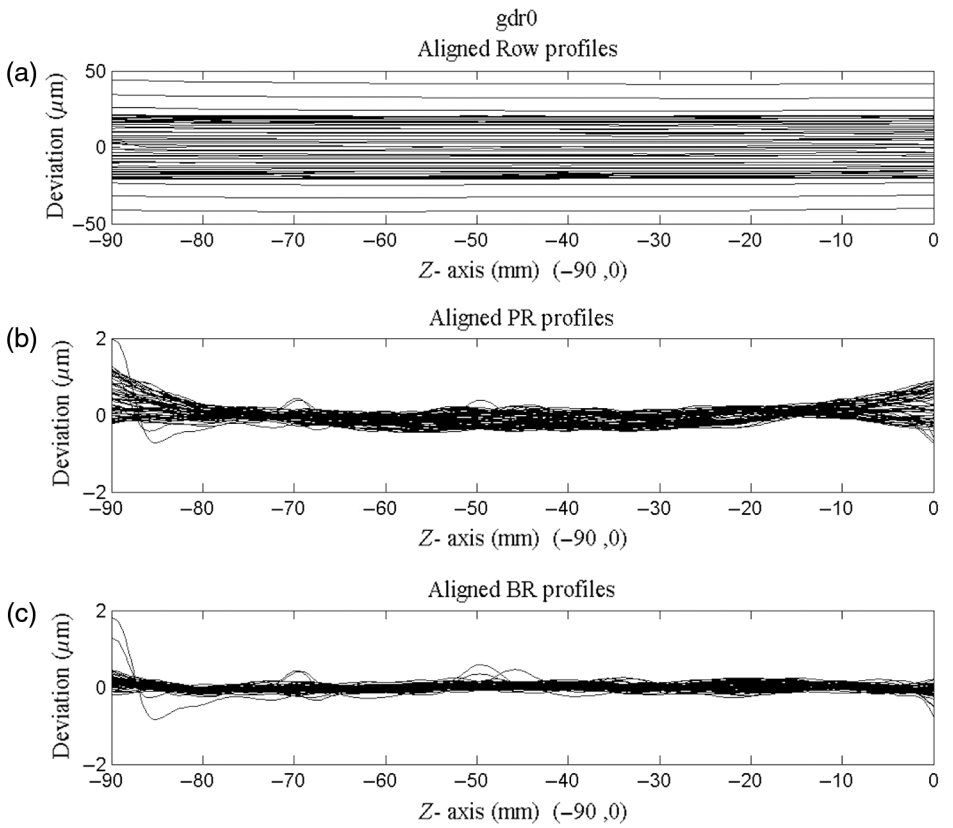

Fig. 3 One-dimensional measurement result by the laser scanner of one of the best mirrors, indicating an HPD of 21″ of the best mirror. (a) The raw data, (b) the aligned phase-removed data, with the azimuthal phase difference removed from the raw data, and (c) the aligned bow-removed data, with the generatrix deviation removed.

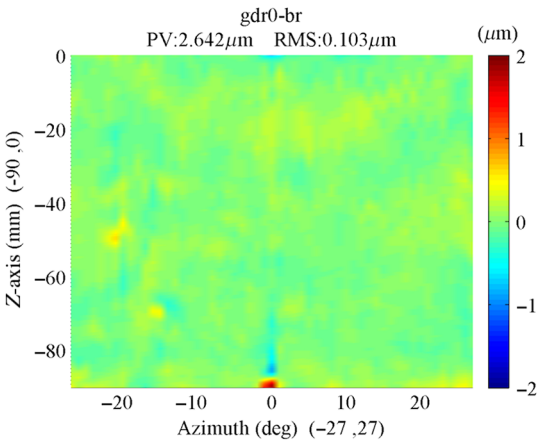

Fig. 4 Two-dimensional measurement result by the laser scanner of one of the best mirrors, indicating a roughness RMS of 0.103 μm.

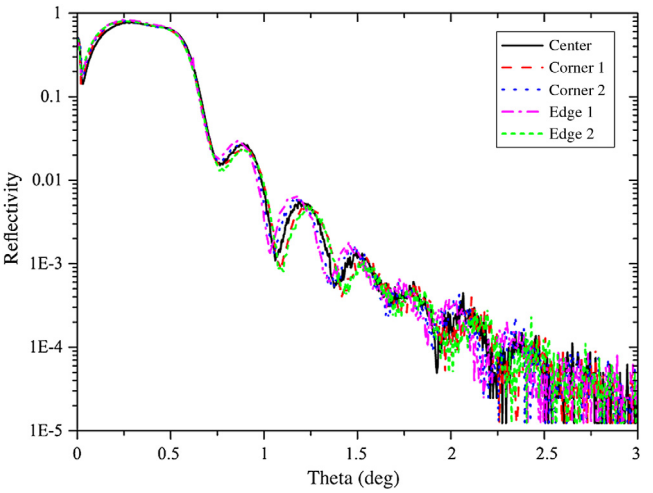

Fig. 5 Uniformity test result at 8.04 keV of samples, coated with 20-nm Pt, which is improved to 3% thus far.

University and specially designed for slumped mirrors' surface quality assessment.[42,43] The slumped mirror surface is scanned by a laser beam, detected by a position-sensitive detector, along the radial direction and axial direction, respectively. By comparing the position between the experimental reflection spot and the theoretical position based on an ideal cylindrical mirror surface, the figure error of the mirror substrate is thus determined. The laser scanner can provide a characterization of the slope error with a precision of $\sim 3''$.

The measurement results of the best mirror are shown in Figs. 3 and 4, one-dimensional and two-dimensional results, respectively. The free-standing mirror substrate is scanned along the axial direction at different azimuthal angles. Figure 3(a) depicts the raw data. Figure 3(b) shows the aligned phase-removed (PR) data, with the azimuthal phase difference removed from the raw data. Figure 3(c) shows the aligned bow-removed (BR) data, with the generatrix deviation removed.[43] Among the measurement results, the aligned BR data are the ultimate results we utilize to assess to mirror quality before assembly process, as shown in Figs. 3(c) and 4. In general, the average of figure accuracy of slumped mirrors improved from over $100''$ in 2016 to $60''$ in 2017 and to $50''$ thus far.

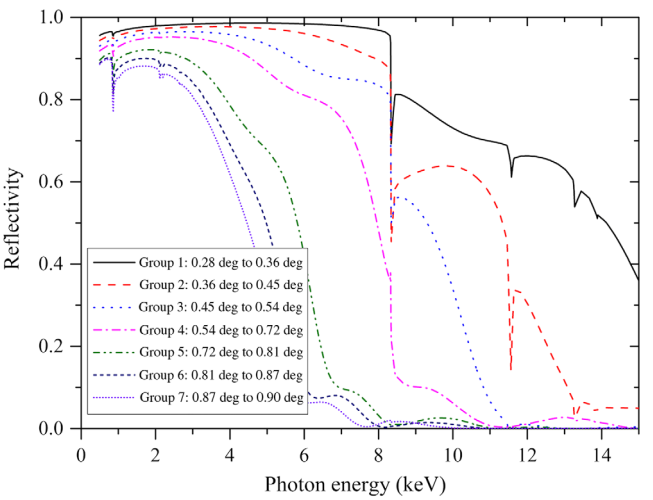

Fig. 6 Reflectivity curves of the coating groups, which are designed for mirror layers with grazing incident angles ranging from 0.28 deg to 0.90 deg.

3 Mirror Coatings

We utilize a dedicated deposition facility, a cylindrical magnetron sputtering coating machine.[44,45] The machine consists of three planar DC magnetron sources toward the outside and several sample holders for mounting the mirror substrates toward the inside, so that it can work for both cylindrical slumped glasses and cylindrical mandrels. Due to its large volume, the coating machine can satisfy the requirement of a large number of mirrors in scheduled time. In addition, the coating thickness is of good uniformity over a cylindrical mirror with 100 mm in length and 60 deg in azimuth, as shown in Fig. 5. The thickness uniformity is improved from about 8% in 2016 to better than 3% now, by measuring the reflectivity of five points on the mirror, one in the center, two in the corner and the other two on the edge.

A set of coatings using C, Ni, and Pt is designed to optimize the effective area, as shown in Fig. 6. Each group of coatings corresponds to a subinterval of grazing angles, with a grazing angle in the range from 0.28 deg to 0.90 deg. The curve of each group in Fig. 6 is the calculated reflectivity at the average incident angle of its range.

The coatings we deposited on the mirrors have the expected high reflectivity, as well as good thermal stability. Here we take the group 2 as an example, which corresponds to angle subinterval from 0.36 deg to 0.45 deg that was deposited on the prototype. The AFM test results in Fig. 7 show a great surface quality, indicating a roughness root mean square (RMS) of 0.3 nm. Meanwhile, the x-ray characterization result at 8.04 keV of the group 2 coatings is shown in Fig. 8, using a roughness RMS of 0.37 nm for fitting. It shows a great agreement with the prediction. Thermal stability test[18] also indicates a good quality of the coatings, by comparing the reflectivity before and after heating the coated mirrors up to 200°C in a vacuum degree of 10^{-4} Pa.

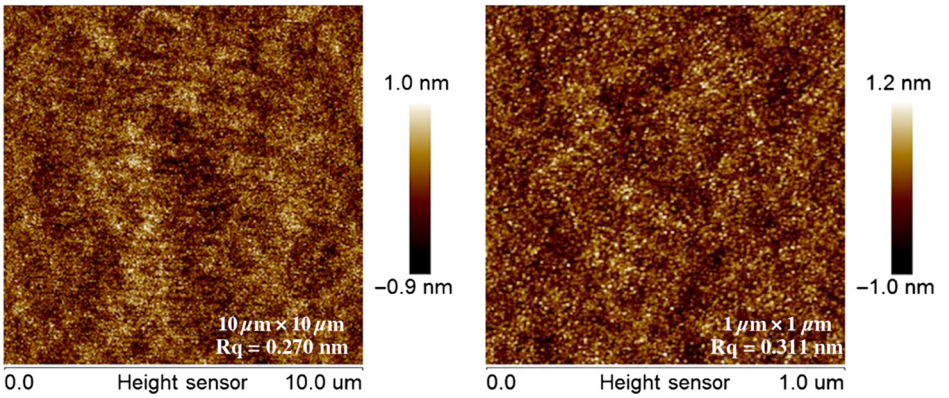

Fig. 7 AFM test results of coating group 2, indicating a roughness RMS of 0.3 nm.

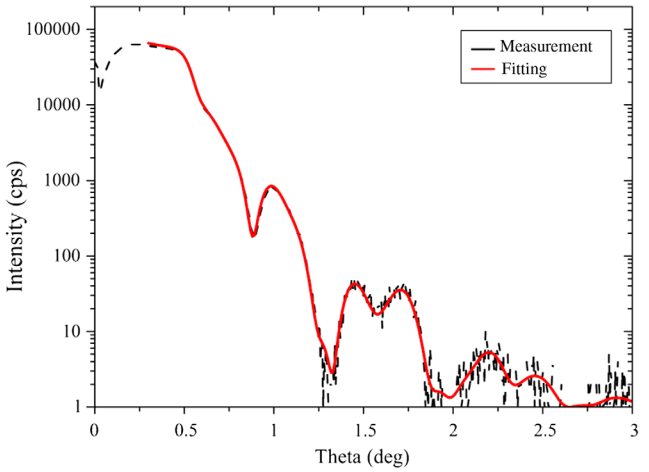

Fig. 8 X-ray characterization result at 8.04 keV of coating group 2, corresponding to a grazing incident angle of 0.36 deg to 0.45 deg.

4 X-Ray Telescope Assembly Technology

During the telescope assembly process, illustrated in Fig. 9, graphite spacers are utilized to build mirrors from the mandrel, operated on an ultraprecise lathe. Graphite spacers and mirrors

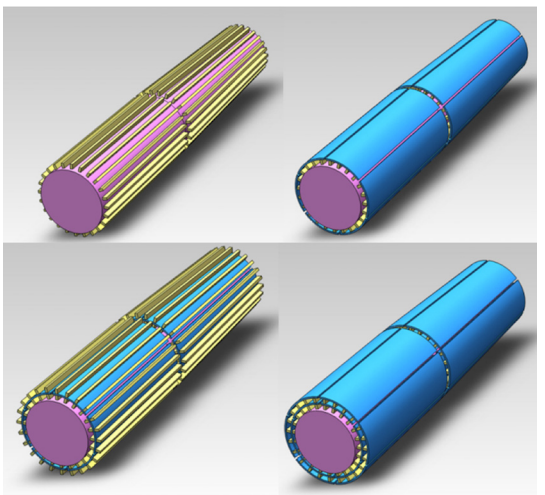

Fig. 9 Illustration of the telescope assembly process. Graphite spacers (the yellow bars) are utilized to build mirrors (the blue shells) from the mandrel (the pink cylinder).

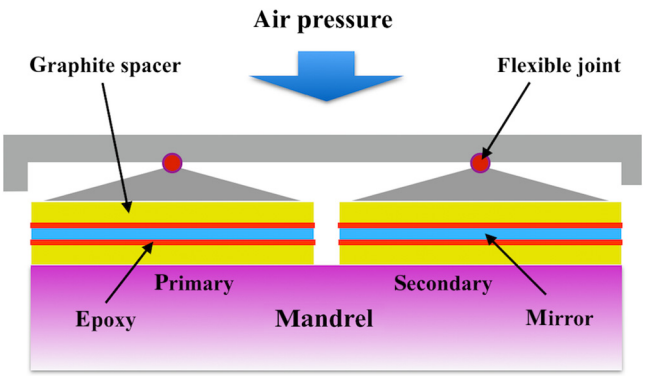

Fig. 10 Illustration of how the mechanical holder works, by means of which the uniform pressure is provided on the primary and secondary mirrors.

are bonded by epoxy. A mechanical holder was designed to optimize the bonding process, which works on the primary and secondary mirrors with air pressure at the same time. Flexible elements and air pressure can provide uniform pressure on the spacers (see Fig. 10).

Metrology plays a very important role in the assembly of the x-ray telescopes. Eligible slumped mirrors are selected by utilizing a laser scanner and interferometer before assembly. The surface deformation of the mirrors introduced during the assembly process will also cause performance degradation in the angular resolution and effective area of x-ray telescopes. Therefore, an *in-situ* measurement system is utilized to measure the mounted mirrors during assembly process. The system includes two kinds of contact mechanical probe, namely, Renishaw 3D touch probe and linear voltage differential transformer (LVDT), and one noncontact optical probe of Precitec Company. The LVDT is an *in-situ* measurement system that is utilized to measure the mounted mirrors during assembly process.[42] The LVDT, a ruby-tipped and capacitive coupled probe with a resolution of 0.1 μm, makes dense azimuthal and axial scans of the mirror segment surface height profile during the prototype assembly. Since the mirror substrates (Schott D263, the same as NuSTAR's) have a good uniformity in thickness, we actually measure the backside of the mounted mirrors. Combining measurements from the three probes makes it possible to determine the shell shape with an accuracy of 0.3 μm. Based on the surface metrology data, optical performance of the

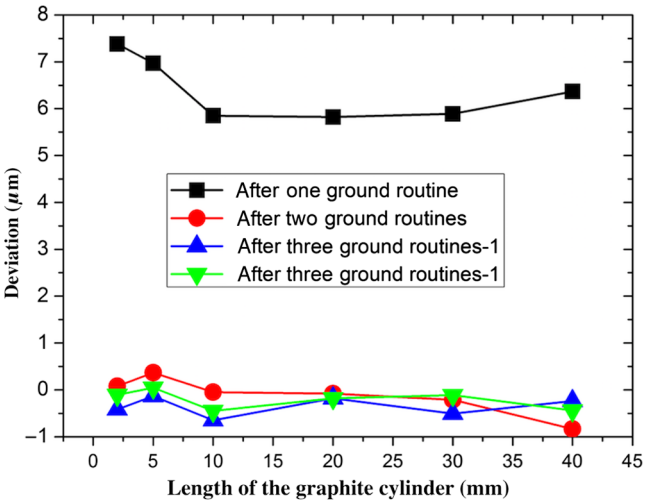

Fig. 11 Measurement results of graphite spacers after the grinding process, indicating that the grinding process provides a submicron knowledge.

optic can be quickly evaluated by means of fitting and the use of a ray-tracing program,[46] thus optimizing the following assembly process. For the next mirror layer assembly, the graphite spacers are grounded by a high-speed grinding wheel. *In-situ* measurement and compensation machining provide the spacers not only with the correct conical angle and straightness but also without the residual error of the previously assembled mirror layer. Submicron knowledge is provided by the grinding process after two grinding routines, as shown in Fig. 11. An extra ground routine is performed to guarantee the spacers a better micro-roughness after two ground routines. Meanwhile, a graphical user interface (GUI) of the program was developed to simplify and facilitate data processing, as shown in Fig. 12.

5 Calibration of the Latest Prototype at PANTER

The latest prototype was tested at the PANTER x-ray test facility,[47,48] which was built to develop and characterize the ROSAT optics. PANTER is characterized by a beam path length of 123.6 m, realized by utilizing a vacuum tube (diameter of 1 m) between the x-ray point source and the instrument chamber (with a length of 12 m and a diameter of 3.5 m). In the chamber, the measurement is performed at a high vacuum degree of $\leq 10^{-4}$ Pa. The long beam path length could provide a wide aperture quasi-parallel x-ray beam, thereby effectively suppressing the effect of the finite source distance over the prototype, of which the nominal focal length f is 2052.5 mm, as shown in Fig. 13.

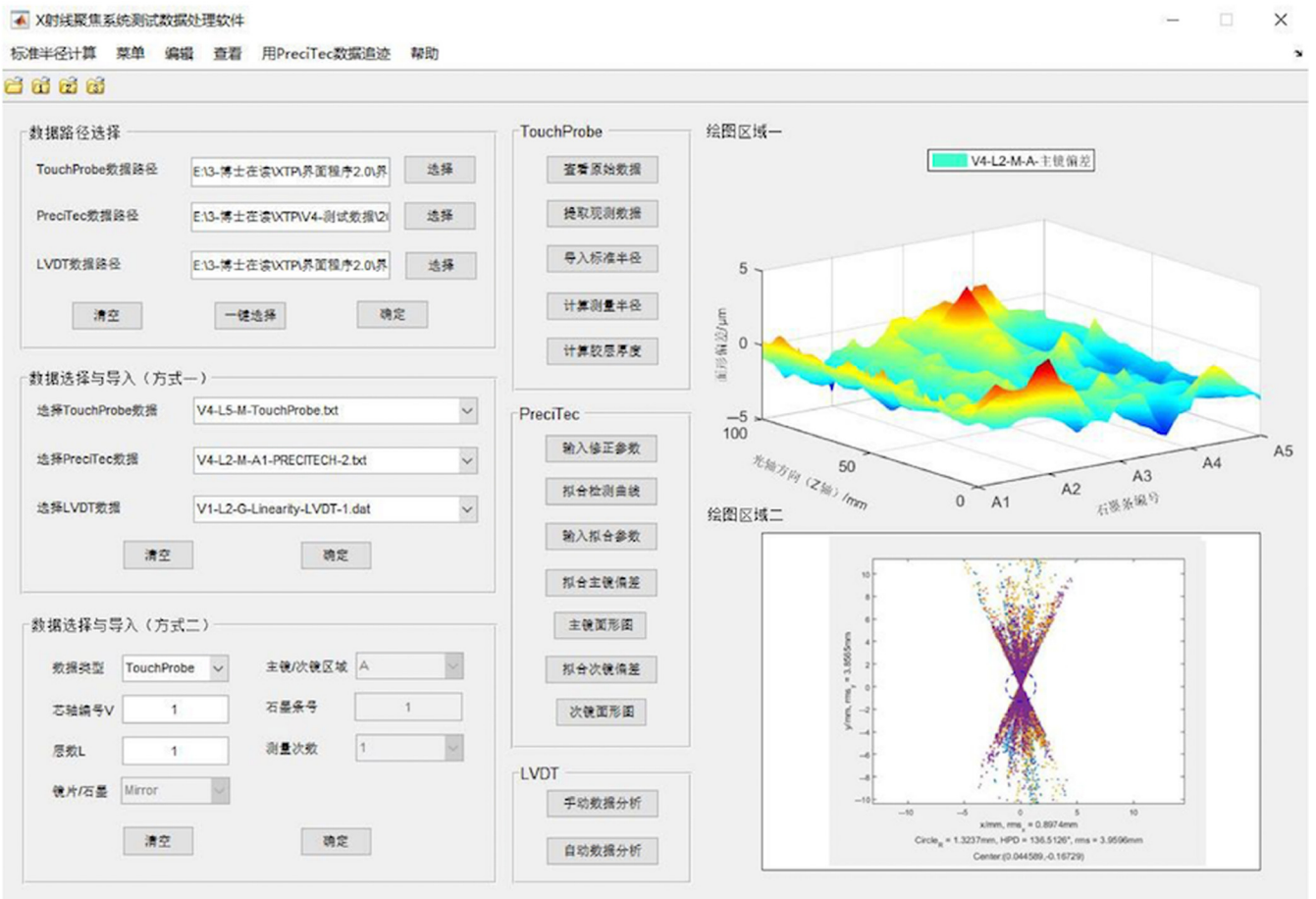

Fig. 12 GUI of the program for data processing, by means of which the assessment of fabricated mirrors in progress is performed based on the *in-situ* measurement.

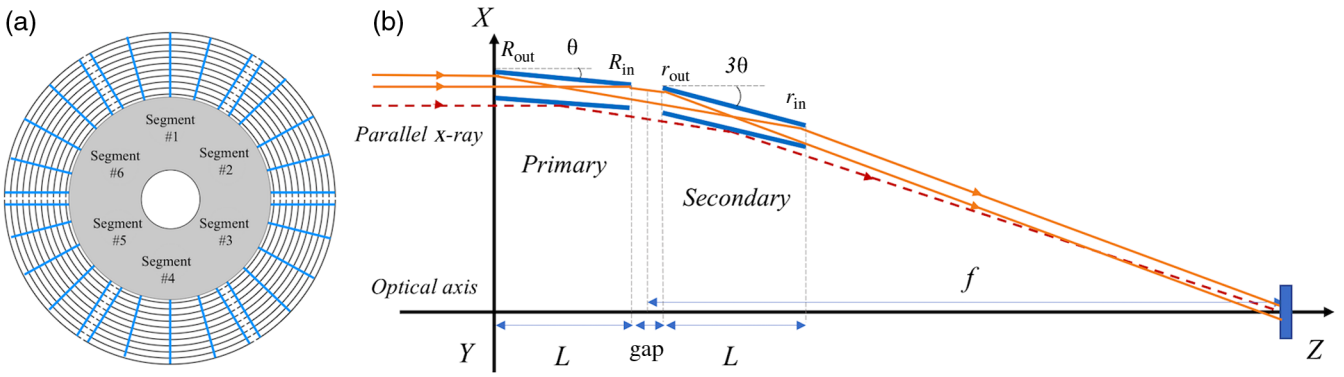

Fig. 13 Schematic representation of the prototype: (a) the entrance aperture and (b) the cross-section profile.

Table 2 Characteristics of the prototype.

Number of layers	21
Focal length f (mm)	2052.5
Diameter D (mm)	104-150
Mirror length L (mm)	100
Mirror thickness t (mm)	0.3
Mirror coating	C/Ni/Pt
Grazing angle θ (deg)	0.365–0.522

5.1 *Latest Prototype with 21 Layers*

The schematic representation of the prototype is shown in Fig. 13, which employs conical Wolter-I configuration. The characteristics are given in Table 2. In the optic, θ is the grazing angle; R_{out} and R_{in} are defined as the radii of the outer edge and the inner edge of the primary mirror and r_{out} and r_{in} are the radii of the outer edge and the inner edge of the secondary mirror, respectively. The gap is the interval between the primary mirror and the secondary mirror, whose axial length is L. To maximize the on-axis collecting area, the 21 mirror layers are tightly nested. The confocal and concentric layers share the common focal length f, which is defined as the axial distance between the focus to the prototype's principal plane. The principal plane is located in the middle between the primary and the secondary conical mirror parts.

Theoretically, in the case of on-axis parallel rays, all rays striking on the primary mirror will be reflected onto the secondary mirror, and then these rays will be converged onto the focal plane without the obscuration resulted from the inner mirrors, as shown in the orange solid lines. In addition, the rays striking on the center of primary mirrors will be reflected onto the center of secondary mirrors, and then converge in the focus, as shown in the red dashed line.

The characteristics of the 21-layer prototype are summarized in Table 2. The preliminary assessment by means of ray-tracing program predicts an angular resolution of 101″ and an effective area of 41 cm^2 at 1.49 keV—our reference energy for the on-axis performance of the prototype. In the simulation, several errors were taken into account, including the 3.9′ divergence of the x-ray beam, the figure error of every individual mirror, and the residual 30″ misalignment after alignment process. The 3.9′ beam divergence is the angular diameter of the incident beam (150 mm in diameter) with respect to the source–optic distance (130,955 mm). The 21-layer prototype consists of six segments, as shown in Fig. 13. Conservatively, 5″ misalignment of the six segments was counted into the angular resolution.

5.2 *Measurement Results*

The prototype was measured at a focal length of 2076 mm, 9-mm deviation from the corrected focal length (2085 mm) for beam divergence, due to the mirror assembly misalignment. Since the knowledge of the on-axis performance of the prototype at 1.49 keV is most important for us, the measured on-axis HPD and effective area at this energy are described in this section. Figure 14 shows the in-focus image and the extrafocal image of the prototype, indicating an HPD of 111″ and an effective area of 39 cm^2 at 1.49 keV. The point spread function measurement is performed at low photon count rate to avoid pile-up, as shown in Fig. 14(a), which requires a long time exposure to accumulate photons. By contrast, the effective area was measured by out-of-focus rings test,[49] as shown in Fig. 14(b), thus preventing the detector from pile-up effects at higher photon count rate. Out-of-focus rings test are performed by moving forward or backward the detector to obtain intrafocal image or extrafocal image.

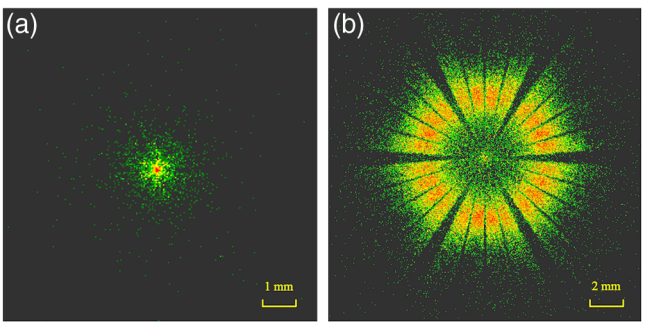

Fig. 14 (a) In-focus image, indicating an HPD of 111″ at 1.49 keV and (b) extrafocal image at a distance of 120 mm from the focal plane, indicating an effective area of 39 cm^2 at 1.49 keV.

Table 3 Measured and simulated effective area.

Energy	Measurement (cm^2)	Simulation (cm^2)	Deviation (%)
525 eV	33	39	18
1.49 keV	39	41	5
4.51 keV	38	40	5
4.95 keV	36	38	6
8.04 keV	23	26	13

The measured HPD is roughly consistent with a simple estimate of the expected HPD of 97″ based on a conical approximation error of ∼35″, an average figure error of ∼60″ (85″ for two reflections), a misalignment between optic and optical axis of ∼30″, and a misalignment between segments of 5″ (by stacking up these errors in quadrature: $\sqrt{35^2 + 2 \times 60^2 + 30^2 + 5^2} \approx 97$). In terms of the figure error, the figure accuracy of the mirrors degraded to some extent after the slumped mirrors are assembled, giving a range of figure errors to be 50″ to 70″. This estimation shows that the conical approximation error is small compared to the figure error, even though it is non-negligible. As we improve the figure accuracy of the mirrors further, the conical approximation error could have more and more significant influence on the imaging quality. Then we could suppress the effect of the conical approximation error by shortening the mirror length or lengthening the focal length.

The effective area at 525 eV, 1.49, 4.51, 4.95, and 8.04 keV were determined, as listed in Table 3, with simulated results for comparison. The reduction in effective area, compared with expectation, is considered as a result of excess epoxy glue. From the extrafocal image in Fig. 14(b), the areas close to the graphite spacers indicate a lower intensity, owing to a little redundant epoxy glue, which spilled out and contaminated the mirrors during epoxy pasting and curing process.

6 Summary

The IXTs have been developed at the IPOE of Tongji University for over a decade. Great improvements have been achieved in the fabrication of the mirrors and coatings, as well as the telescope assembly. Most of mirror substrates have a decent figure accuracy of 30″ to 60″ by thermal slumping technology, and the best one has an HPD of 21″. The coatings are characterized by a roughness RMS of 0.3 nm, as well as expected high reflectivity and good thermal stability. In addition, the *in-situ* measurement system and three-dimensional ray-tracing program were developed to guide the telescope assembly process, providing a high reliability. Furthermore, the latest prototype with 21 layers was calibrated at the PANTER x-ray test facility, indicating an HPD of 111″ and effective area of 39 cm^2 at 1.49 keV.

Acknowledgments

This work was supported by the National Natural Science Foundation of China (Nos. U1731242, 61621001, and 11873004) and Strategic Priority Research Program of the Chinese Academy of Sciences (Nos. XDA15010400 and XDA04060605).

References

1. V. H. Wolter, "Spiegelsysteme streifenden Einfalls als abbildende Optiken für Röntgenstrahlen," *Ann. Phys.* **445**(10), 94–114 (1952).
2. R. Giacconi and B. Rossi, "A telescope for soft x-ray astronomy," *J. Geophys. Res.* **65**(2), 773–775 (1960).
3. L. P. VanSpeybroeck and R. C. Chase, "Design parameters of paraboloid-hyperboloid telescopes for x-ray astronomy," *Appl. Opt.* **11**(2), 440–445 (1972).
4. R. Petre and P. J. Serlemitsos, "Conical imaging mirrors for high-speed x-ray telescopes," *Appl. Opt.* **24**(12), 1833–1837 (1985).
5. P. J. Serlemitsos, "Conical foil x-ray mirrors: performance and projections," *Appl. Opt.* **27**(8), 1447–1452 (1988).
6. W. Werner, "Imaging properties of Wolter I type x-ray telescopes," *Appl. Opt.* **16**(3), 764–773 (1977).
7. P. L. Thompson and J. E. Harvey, "Development of an imaging performance criterion for wide-field grazing incidence x-ray telescopes," *Proc. SPIE* **3766**, 162–172 (1999).
8. T. T. Saha et al., "Optical design for a survey x-ray telescope," *Proc. SPIE* **9144**, 914418 (2014).
9. M. C. Weisskopf, "Chandra x-ray optics," *Opt. Eng.* **51**(1), 011013 (2012).
10. D. H. Lumb et al., "X-ray multi-mirror mission (XMM-Newton) observatory," *Opt. Eng.* **51**(1), 011009 (2012).
11. F. A. Harrison et al., "The nuclear spectroscopic telescope array (NuSTAR) high-energy x-ray mission," *Astrophys. J.* **770**, 103 (2013).
12. T. Li et al., "Insight-HXMT observations of the first binary neutron star merger GW170817," *Sci. China-Phys. Mech. Astron.* **61**(3), 031011 (2017).
13. Y. Dong, "The x-ray timing and polarization satellite—1, 2, 3: uncovering the mysteries of black holes and extreme physics in the universe," *Proc. SPIE* **9144**, 91443O (2014).
14. S. N. Zhang et al., "eXTP: enhanced x-ray timing and polarization mission," *Proc. SPIE* **9905**, 99051Q (2016).
15. W. Yuan et al., "Einstein probe—a small mission to monitor and explore the dynamic x-ray universe," *Huazhong Univ. Sci. Technol. J.* **23**(4), 383 (2015).
16. Z. Wang et al., "Development of the x-ray timing and polarization telescope optics," *Proc. SPIE* **9144**, 91441E (2014).
17. Z. Shen et al., "Development of x-ray multilayer telescope optics for XTP mission," *Proc. SPIE* **9905**, 990520 (2016).
18. Z. Shen et al., "Current progress of x-ray multilayer telescope optics based on thermally slumping glass for eXTP mission," *Proc. SPIE* **10699**, 106991B (2018).
19. S. E. Labov, "Figured grazing incidence mirrors from reheated float glass," *Appl. Opt.* **27**(8), 1465–1469 (1988).
20. S. Chen et al., "Wolter-I-like x-ray telescope structure using one conical mirror and one quadric mirror," *Chin. Opt. Lett.* **14**(12), 123401–123405 (2016).
21. Y. Liao et al., "Design of conical Wolter-I geometry with sectioned secondary mirrors for x-ray telescopes," *J. Astron. Telesc. Instrum. Syst.* **5**(1), 014004 (2019).
22. G. Matthews and K. Havey, "Ten years of Chandra: reflecting back on engineering lessons learned during the design, fabrication, integration, test, and verification of NASA's great x-ray observatory," *Proc. SPIE* **7738**, 77380Y (2010).
23. B. Aschenbach, "Design, construction, and performance of the ROSAT high-resolution x-ray mirror assembly," *Appl. Opt.* **27**(8), 1404–1413 (1988).
24. R. Giacconi et al., "The Einstein/HEAO 2/x-ray observatory," *Astrophys. J.* **230**, 540–550 (1979).
25. Y. Soong, L. Jalota, and P. J. Serlemitsos, "Conical thin foil x-ray mirror fabrication via surface replication," *Proc. SPIE* **2515**, 64–69 (1995).
26. P. J. Serlemitsos et al., "The x-ray telescope onboard Suzaku," *Astron. Soc. Jpn.* **59**, S9–S21 (2007).
27. T. Takahashi et al., "The ASTRO-H x-ray observatory," *Proc. SPIE* **8443**, 84431Z (2012).
28. E. Balsamo et al., "Concept study x-ray testing for NICER's x-ray concentrators," *Proc. SPIE* **8861**, 88611M (2013).
29. G. Pareschi et al., "Development of grazing-incidence multilayer mirrors by direct Ni electroforming replication: a status report," *Proc. SPIE* **5900**, 590008 (2005).

30. M. P. Ulmer et al., "The fabrication of Wolter I multilayer coated optics via electroforming: an update," *Proc. SPIE* **3773**, 113–121 (1999).
31. O. Citterio et al., "Optics for the x-ray imaging concentrators aboard the x-ray astronomy satellite SAX," *Appl. Opt.* **27**(8), 1470–1475 (1988).
32. N. Gehrels et al., "The swift gamma-ray burst mission," *Astrophys. J.* **611**, 1005–1020 (2004).
33. P. Friedrich et al., "Design and development of the eROSITA x-ray mirrors," *Proc. SPIE* **7011**, 70112T (2008).
34. W. W. Zhang et al., "Development of lightweight x-ray mirrors for the constellation-X mission," *Proc. SPIE* **5488**, 820–828 (2004).
35. W. W. Craig et al., "Fabrication of the NuSTAR flight optics," *Proc. SPIE* **8147**, 81470H (2011).
36. M. J. Collon et al., "Silicon pore optics for the ATHENA telescope," *Proc. SPIE* **9905**, 990528 (2016).
37. R. E. Riveros et al., "Fabrication of high resolution and lightweight monocrystalline silicon x-ray mirrors," *Proc. SPIE* **9603**, 96030W (2015).
38. J. A. Gaskin et al., "The lynx x-ray observatory: concept study overview and status," *Proc. SPIE* **10699**, 106990N (2018).
39. R. S. McClelland, "The STAR-X x-ray telescope assembly (XTA)," *Proc. SPIE* **10399**, 1039908 (2017).
40. S. Ma et al., "Thermal stability and separation characteristics of anti-sticking layers of Pt/Cr films for the hot slumping technique," *Chin. Phys. C* **40**(7), 079001 (2016).
41. W. W. Zhang, "Manufacture of mirror glass substrates for the NUSTAR mission," *Proc. SPIE* **7437**, 74370N (2009).
42. J. E. Koglin et al., "First results from the ground calibration of the NuSTAR flight optics," *Proc. SPIE* **8147**, 81470J (2011).
43. M. A. Jimenez-Garate, W. W. Craig, and C. J. Hailey, "Fast optical metrology of the hard x-ray optics for the high energy focusing telescope (HEFT)," *Proc. SPIE* **3444**, 622–633 (1998).
44. R. Qi et al., "Effects of sputtering parameters and separator plates on the structure and stress of W/Si multilayers in x-ray telescope applications," *Opt. Eng.* **56**(3), 035103 (2017).
45. R. Qi et al., "Stress and microstructure study of W/Si x-ray multilayers with different structural parameters," *J. Nanosci. Nanotechnol.* **19**(1), 568–574, (2019).
46. J. Yu et al., "Ray tracing method for the evaluation of grazing incidence x-ray telescopes described by spatially sampled surfaces," *Appl. Opt.* **57**(7), B74–B82 (2018).
47. M. J. Freyberg et al., "The MPE X-ray test facility PANTER: calibration of hard x-ray (15–50 keV) optics," *Exp. Astron.* **20**, 405–412 (2006).
48. M. J. Freyberg et al., "New technology and techniques for x-ray mirror calibration at PANTER," *Proc. SPIE* **7011**, 701117 (2008).
49. K. Misaki et al., "X-ray characterization of eROSITA mirror shells using out-of-focus images," *Proc. SPIE* **7011**, 70112Z (2008).

Zhanshan Wang is a SPIE fellow and a professor in Tongji University. He received his MS degree in optics from Changchun Institute of Optics and Fine Mechanics, CAS, in 1988, and His PhD in optics from Shanghai Institute of Optics and Fine Mechanics, CAS, in 1996. He is the author of more than 150 journal papers. His current research interests include soft x-ray sources, optics in extreme ultraviolet and x-ray region, optical coatings for lasers and optical systems.

Biographies of the other authors are not available.